RESEARCH

Mechanics of confined swelling in hydrogels

Silvia Monchetti[1] · Farzad Tatar[2] · Michele Betti[1] · Roberto Brighenti[1]

Received: 8 September 2025 / Revised: 26 November 2025 / Accepted: 5 February 2026

Abstract
Hydrogels are stimuli responsive materials whose physical–chemical-mechanical properties and responsiveness are tunable; their behavior is similar to those observed in natural living tissues, and their use is promising in a wide range of applications, especially in the biomedical field. In the present study, we investigate experimentally and provide a theoretical interpretation of the swelling phenomenon, both in free (i.e. without constraints) and confined 1-D and 2-D conditions, of poly(acrylamid-co-acrylic acid) hydrogels, in terms of volume ratio increase, of the Flory–Huggins interaction parameter, and the stress state arising in the network. Relying on a theoretical multi-physics-based theory describing fluid diffusion, and mechanics, the swelling process is interpreted and quantitatively discussed, providing new insights in the realm of controlled swelling of hydrogels for their exploitation in new and advanced applications.

Keywords Hydrogels · Confined swelling · Chemical potential · Mechanics of swelling · Osmotic pressure

Abbreviations

A_n	Avogadro's constant
b	Kuhn's length of a chain segment
C_s	Solvent's concentration in the reference state
c_s	As before but referred to the current configuration
D	Diffusion coefficient
$\boldsymbol{E}$	Green–Lagrange deformation tensor
$\boldsymbol{F}$	Deformation gradient tensor
G	Shear modulus
k_B	Boltzmann constant
$J = 1 + C_s v_s$	Volume ratio
J_c	Volume ratio for constrained swelling
$\boldsymbol{j}$	Solvent flux vector
m_0	Initial mass of the spherical gel beads
n	Number of hydrogel's cross-linked chains per unit volume
N	Number of segments in a polymer chain belonging to a single network
p_{atm}	Atmospheric pressure
p_o	Hydrostatic osmotic pressure
p	Cauchy hydrostatic stress
$\boldsymbol{P}$	First Piola stress tensor
$\boldsymbol{s}$	Cauchy deviatoric stress tensor
t	Time

Published online: 25 March 2026

 https://doi.org/10.1007/s11012-026-02095-6

T	Absolute temperature
v_s	Fluid molar volume
χ	Flory–Huggins parameter governing the swelling phenomenon
δ	Confining distance
ϕ_0, ϕ	Initial (dry) and final (swollen) diameter of the spherical hydrogel element, respectively
λ	Macroscopic stretch
μ	Chemical potential
ψ_{gel}	Gel's energy density
ψ_{net}, ψ_p	Network's deformation energy density and energy density due to the hydrostatic pressure p in the network
ψ_{mix}	Polymer-fluid mixing energy density
ψ_{ext}	Mechanical energy density associated to external forces
$\boldsymbol{\sigma}$	Chauchy stress tensor
ω	Deformation function
$\Omega(\partial\Omega), \Omega_0(\partial\Omega_0)$	Omain of a continuum body and its boundary, in the reference and current configuration, respectively

1 Introduction

Hydrogels are made by a three-dimensional polymer network capable of absorbing and retaining large amounts of water, without dissolving in it, because of their hydrophilic character [1–6]. Thanks to their high water content and softness, hydrogels are good candidate to mimic the physical characteristics of natural materials, such as biological tissues, making them highly attractive for a wide range of biomedical and engineering applications [7–11].

Hydrogels can be synthesized from natural polymers (e.g., alginate, gelatin, hyaluronic acid) or synthetic polymers (e.g., polyethylene glycol (PEG), polyacrylamide), and their properties—such as porosity, mechanical strength, and degradation—can be tailored through chemical or physical crosslinking.

Recent advancements have been made in the use of hydrogels in the field of art conservation, to overcome the limitations of traditional restoration materials; their use has been proven to be effective in consolidation, cleaning, and protection of works of art, especially of paintings where the use of environmentally-friendly technologies using low-toxicity materials is particularly sought for. As a matter of fact, the exploitation of these advanced materials calls for a comprehensive knowledge of their mechanical behavior and of the interaction with different substrates and surfaces as well as their in-situ responsiveness to external and environmental stimuli [12–14]. Tunable size, stiffness or surface properties, make these materials particularly suitable for a variety of applications. The combination of microgels and nanostructured fluids for a novel cleaning system which aims to extend the application of soft matter materials in the field of cultural heritage is explored in [15]. Another study underlines that the cleaning performance of hydrogels is influenced by the surface roughness and provided new insights into the structure–function relationship of gels for cultural heritage conservation [16, 17]. As a matter of fact, understanding the behavior of hydrogels under constraints offers relevant insights to increase the knowledge about the mechanisms taking place in these situations to be exploited in application where the gel deformation is constrained by the surrounding media, such as in applications devoted to art conservation. The principles governing 1-D or 2-D confined swelling are directly applicable to conservation purposes, where controlled expansion of gels is used to lift contaminants without damaging underlying artistic substrates as well as for removing soil, aged coatings, and overpaints in art restoration. In particular, the volumetric change of gel-based cleaning systems have been investigated to modulate adhesion, solvent release, and mechanical action on heterogeneous substrates [17].

Similarly, in the biomedical field jammed microgels have been developed as tailored inks for 3D printing, showing how rheology, stability, and functionality can be tailored at will [18]. The hydrogel versatility is thus

evidenced across disciplines, where their tunable structure–property relationship enables applications ranging from cultural assets conservation to advanced biomedical technologies.

While free swelling, i.e. taking place without any external mechanical constraint, has been extensively investigated, most practical applications involve swelling under constraints and confinements. In practice, boundaries such as rigid walls, porous structures, or neighbouring tissues can interact with the volume expansion mechanism of swelling, generating contact stresses, and influencing the performance of the material, so making confinement a key factor in hydrogel design. In this framework, the present paper aims to enhance the study of the hydrogels response by comparing the emerging volume ratio and their mechanics in free swelling conditions with the confined ones.

The topic relevance is well established in the scientific literature [19–24]. For instance, thin films made of smart hydrogels used as pressure-generating materials and the functional effects of confinement in chemo-mechanical sensors have been investigated in [19]. Another study has shown how hydrogels swelling is modified by the presence of obstacles which alter the geometry of their shape evolution and has identified the specific conditions causing fracture failure [20]. Swelling of hydrogels interacting with rigid and elastic confinements has been investigated in [21] where it has been shown that the equilibrium configuration of a gel swelling under constraint depends on the geometry of the confinement, the degree of swelling, and the stiffness of the applied constraint. In [22], inspired by phenomena observed in nature, interesting theoretical and experimental results concerning the locomotion in confined spaces have been provided; specifically, a channel-like confinement has been considered and self-motility has been proven by using temperature-sensitive hydrogel, showing motion capabilities similar to those observed by larvae and worms. Swelling-strengthening of polymers obtained by a bioinspired strategy, harnessing membrane nanobarriers for regulating transmembrane fluid transport, has been studied in [23], while controlled swelling through a properly designed elastic confinement has been considered in [24].

The present study analyzes experimentally the swelling phenomenon in both free and 1-D and 2-D confined conditions, of poly(acrylamid-co-acrylic acid) hydrogels; volume ratio evolution and stress state arising in the network are quantified for different degree of confinements. By using a theoretical multi-physics-based framework describing fluid diffusion, and mechanics, the swelling process is analytically described in the steady state condition and quantitatively discussed, providing new insights in the realm of controlled swelling with potential implications for both fundamental science and application-oriented design. The present study aims at providing detailed quantitative information on hydrogel swelling under 1-D and 2-D confinements, understanding how the swelling process evolves in presence of constraints, and what is the pressure exerted by the gel on the surrounding confining environment. We consider the swelling phenomenon—during its evolution from the dry state up to the final steady state condition—in free as well as in constrained conditions; the Flory–Huggins parameter is evaluated vs the relative size of the constraining region, while the contact area and the contact stress are evaluated experimentally; further, a simple theoretical model is proposed to assess the contact stress in both 1-D and 2-D confined swelling conditions. These findings represent a fundamental knowledge for the precise design of gel-based devices whose swelling is controllable by playing with the surrounding constraints.

The paper is organized as follows: Sect. 2 briefly illustrates the mechanics of free swelling in hydrogels, while Sect. 3 deals with the same problem but for confined gels. Section 4 presents the experimental tests performed for quantifying the main physical–mechanical aspects involved in free (Sect. 4.1) and confined (Sect. 4.2) swelling. Section 5 closes the paper by discussing the obtained results and providing future research perspectives related to exploitation possibilities of controlled swelling.

 https://doi.org/10.1007/s11012-026-02095-6

2 Mechanics of swelling in hydrogels

The hydrogel's microstructure is constituted by entangled linear chains, joined at cross-link sites to form a complex network, permeated by a water phase whose molecules can migrate inside the network [25–30]. The network does not interact chemically with the solvent, so the hydrogel microstructure maintains its physical stability; after a transient phase in which the solvent diffuses into the network, and an equilibrium state between the stretched network and the pressure in the fluid, according to the involved thermodynamic forces, is reached.

It is common practice to assume the polymer network and the fluid to be individually incompressible, so the volume increase of the hydrogel taking place upon swelling, corresponds exactly to the volume of the incoming fluid. Let $\boldsymbol{X}$ denotes a generic point in the initial configuration Ω_0 (volume V_0) with boundary $\partial\Omega_0$ (surface area A_0); the deformed configuration is described by $\chi_d(\boldsymbol{X})$ mapping the initial domain Ω_0 to the current one Ω (with volume V) with boundary $\partial\Omega$ (having area A). The deformation gradient tensor is $\boldsymbol{F} = 1 + \partial\chi_d(\boldsymbol{X})/\partial\boldsymbol{X}$, 1 being the second order unit tensor. The fluid balance equation at a generic time instant is given by:

$$\frac{\partial C_s}{\partial t} - \nabla \cdot \boldsymbol{J} = 0 \tag{1}$$

Equation (1) states that the time rate of the fluid concentration $\partial C_s/\partial t$ is equal to the divergence of the vector flux $\boldsymbol{J}$ of the fluid crossing any generic infinitesimal reference volume within the gel domain per unit time (positive if entering into the volume, Fig. 1).

The volume change ratio of the hydrogel is given by $J = V/V_0 = \det\boldsymbol{F}$, and the fluid concentration in the current (c_s) and in the reference (C_s) configuration are related as follows: $c_s = C_s/\det\boldsymbol{F}$. Recalling that the volume increase comes only from the fluid incoming into the network, at any time t it happens to be $J(t) = \det\boldsymbol{F}(t) = 1 + C_s(t)v_s$, being v_s is the molar volume of the fluid that, in the case of water, is equal to $v_s = 1.801 \cdot 10^{-5} m^3/mol$, while C_s is the fluid concentration per unit initial volume of the gel.

The network-fluid equilibrium state corresponds to a condition of minimum energy of the system which is achieved when a given amount of fluid has entered into the network. The fluid concentration is typically considered to be a function of the chemical potential μ and of the osmotic pressure p_o [31–33]; accordingly, the fluid concentration rate can be written: $\dot{C}_s = \frac{\partial C_s(\mu,p)}{\partial t} = \frac{\partial C_s}{\partial \mu}\dot{\mu} + \frac{\partial C_s}{\partial p}\dot{p}_o$, where $\dot{\blacksquare} = \partial\blacksquare/\partial t$ indicates the time derivative.

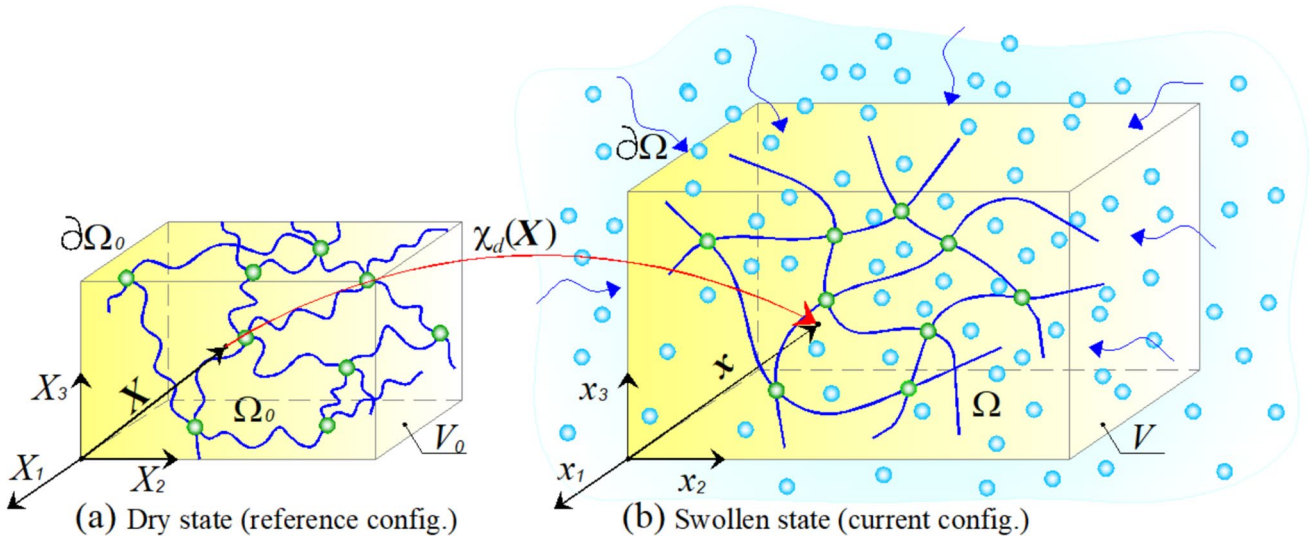

Fig. 1 Schematic of the fluid diffusion within a hydrogel network. Reference dry state (**a**) and swollen state (**b**)

The equilibrium state of the system corresponds to the osmotic pressure balancing the stress state in the network due to the stretch induced by the fluid uptake and, if it is the case, by the external forces applied to the hydrogel. In other words, the gel keeps swelling until the fluid concentration enables fulfilling such a stress balance. By adopting the Fick's law to express the fluid flux-chemical potential gradient relationship [29, 31], $\boldsymbol{J} = -\boldsymbol{M}_L \nabla \mu$, being $\boldsymbol{M}_L = \boldsymbol{D}\left(k_B' T\right)^{-1}$ the mobility tensor (with $\boldsymbol{D}$ the diffusivity tensor) quantifying how easily the solvent diffuses inside the hydrogel network, the balance Eq. (1) becomes:

$$\begin{aligned} &\left[\frac{\partial C_s}{\partial \mu}\dot{\mu} + \frac{\partial C_s}{\partial p}\dot{p}_o\right] + \boldsymbol{M}_L \nabla^2 \mu = 0 \\ &\frac{\partial C_s}{\partial t} - \nabla \cdot \boldsymbol{J} = 0 \end{aligned} \tag{2}$$

being D, T the diffusion coefficient and the absolute temperature, respectively, while $k_B\prime = k_B A_n$, where k_B, and A_n are the Boltzmann constant and Avogadro's number, respectively.

The free energy density of the hydrogel ψ_{gel} is expressed as the sum of a mechanical one ψ_m and the osmotic pressure-related term ψ_p [26]:

$$\psi_{gel} = \psi_m\left(\boldsymbol{F}, C_s\right) + \psi_p\left(J, C_s\right) = \left[\psi_{net}(\boldsymbol{F}) + \psi_{mix}\left(C_s, T\right)\right] + p\left[\left(1 + v_s C_s\right) - J\right] \tag{3}$$

being $p = p_o - p_{atm}$ the effective osmotic pressure of the fluid in the gel when the atmospheric pressure is taken into account; as a matter of fact, the role of the p_{atm} results to be not negligible in extremely deformable solids such as in gels.

The mechanical energy density has been written as $\psi_m = \psi_{net} + \psi_{mix}$, with ψ_{net} the network deformation energy, and ψ_{mix} the polymer–solvent mixing energy which, in general, can be a function of the temperature; however, this dependence will be neglected in the rest of the study. The last term in Eq. (3) comes from the volume constraint $J = 1 + C_s v_s \geq 1$, and the hydrostatic osmotic pressure p plays the role of an internal stress state enforcing the above-mentioned volume constraint.

At the equilibrium, the variation of the total energy evaluated over the volume V, $\Psi_{gel} = \Psi_m + \Psi_p + \Psi_{ext}$ (where the energy Ψ_{ext} associated with the external body $\boldsymbol{b}$ and traction $\boldsymbol{t}$ forces has been included), must vanish [30, 31]; in the current swollen configuration this variational statement reads:

$$\begin{aligned} \delta\Psi_{gel} &= \delta \int_V \psi_{gel} dV \\ &= \int_V \left[\frac{\partial \psi_{net}\left(\boldsymbol{F}, C_s\right)}{\partial \boldsymbol{E}} : \delta\boldsymbol{E} + p\frac{\partial J}{\partial \boldsymbol{E}} : \delta\boldsymbol{E} + \left(\frac{\partial \psi_{mix}\left(C_s\right)}{\partial C_s} + p v_s\right)\delta C_s\right] dV \\ &+ \delta \int_V \psi_{ext}(\boldsymbol{b})\, dV + \delta \int_A \psi_{ext}(\boldsymbol{t})\, dA \\ &= \int_V \left[\left(\boldsymbol{S} + \boldsymbol{F}^{-1} p J \boldsymbol{F}^{-T}\right) : \delta\boldsymbol{E} + \left(\mu + p v_s\right)\delta C_s\right] dV \\ &- \left(\int_V \boldsymbol{b} \cdot \delta\boldsymbol{u}\, dV + \int_A \boldsymbol{t} \cdot \delta\boldsymbol{u}\, dA\right) = 0 \end{aligned} \tag{4}$$

where $\boldsymbol{S} = \frac{\partial \Psi_{net}\left(\boldsymbol{F}, C_s\right)}{\partial \boldsymbol{E}} = \boldsymbol{F}^{-1}\boldsymbol{P}$ is the second Piola–Kirchhoff (P-K) stress tensor (while $\boldsymbol{P}$ is the first P-K stress tensor), $\boldsymbol{E}$ is the Green–Lagrange deformation tensor, and $\delta\boldsymbol{u}$ represents the virtual displacement field. The so-called chemical potential μ appearing in Eq. (4) is the derivative of the mixing energy with respect to the solvent

concentration, $\mu = \partial\psi_{mix}/\partial C_s$. It is worth noticing that the term $(\mu + pv_s)$ in Eq. (4) represents the total chemical potential (or specific Gibbs free energy) of the solvent component when pressure is accounted for. The osmotic pressure p modifies the chemical potential when mechanical work is done on the system and its effect consists in hindering the fluid molecules to enter into the network.

When no external forces are present, at the steady state no fluid motion exist within the gel's network, i.e. $\boldsymbol{J} = \nabla\mu = 0$ and the fluid concentration does not change anymore, $\dot{C}_s = 0$; accordingly, the equilibrium condition reduces to $\boldsymbol{P} = \boldsymbol{FS} = pJ\boldsymbol{F}^{-T}$ in the reference configuration or $\boldsymbol{\sigma} = p\boldsymbol{1}$ in the current configuration, i.e. the elastic stress balances the effective osmotic pressure $p = p_o - p_{atm}$; the atmospheric pressure p_{atm} has to be accounted for since it plays a role for extremely deformable gels.

The network-fluid mixing energy Ψ_{mix} in Eq. (3) is usually expressed as [1, 28]:

$$\Psi_{mix} = \frac{k_B\prime T}{v_s} \cdot \left[(J-1)\ln\left(\frac{v_s C_s}{J}\right) + v_s C_s \frac{\chi(C_s)}{J} \right] \tag{5}$$

where the so-called network-fluid affinity, quantified by the Flory–Huggins interaction parameter χ, has been introduced.

In polymer physics, it is common practice to assume the affine deformation hypothesis, so the deformation energy of the network can be expressed by using the macroscopic deformation gradient tensor $\boldsymbol{F}$ as follows [31]:

$$\Psi_{net}(\boldsymbol{F}) = G\left[tr\left(\boldsymbol{FF}^T\right) - 3 - 2\ln J\right] = \frac{1}{2} nK_B T\left[\lambda_1^2 + \lambda_2^2 + \lambda_3^2 - 3 - 2\ln\left(\lambda_1\lambda_2\lambda_3\right)\right] \tag{6}$$

where the second expression in Eq. (6) has been written by referring to the principal stretch directions (being $\lambda_1, \lambda_2, \lambda_3$ the principal stretches), while n represents the number of cross-linked chains per unit volume [34, 35].

3 Mechanics of confined swelling

Swelling is driven primarily by the osmotic pressure, which arises because the material contains solutes that attract the solvent (water in case of hydrogels). Confined swelling occurs when the gel expansion due to fluid absorption takes place in presence of mechanical obstacles, or constraints interacting with the gel itself. Differently from free swelling where the material expands uniformly in all directions, in confined swelling the mechanical constraints limit the deformation of the material and generate further internal stresses, beyond those due to chains stretch induced by water uptake.

If the applied constraints are too severe, such as when the gel is forced to swell in a narrow confining environment limiting the deformation in one or two directions, gel failure could take place due to the excessively large stress arising along the unconstrained directions.

In the present study we consider the problem of a spherical gel bead expanding freely (Fig. 2a) or in presence of a 1-D or 2-D confinement; in the first case, two rigid parallel planes placed at a fixed distance δ are considered (Fig. 2b, swelling constrained in the X_2 direction), while in the second case a tube with a square cross section with size δ is adopted to limit swelling along two directions at the same time, namely X_1, X_2 (Fig. 1c).

It is worth recalling that the elastic property of a swollen spherical gel element can be evaluated through a simple compression test, where the force–displacement relationship can be determined by using the relation between the applied force P and the diameter reduction (quantified by the displacement u) of an Neo-Hookean sphere with diameter ϕ and Poisson's ratio ν, can be written in the form:

$$P = G\phi^2 F\left(\frac{2u}{\phi}\right) \tag{7}$$

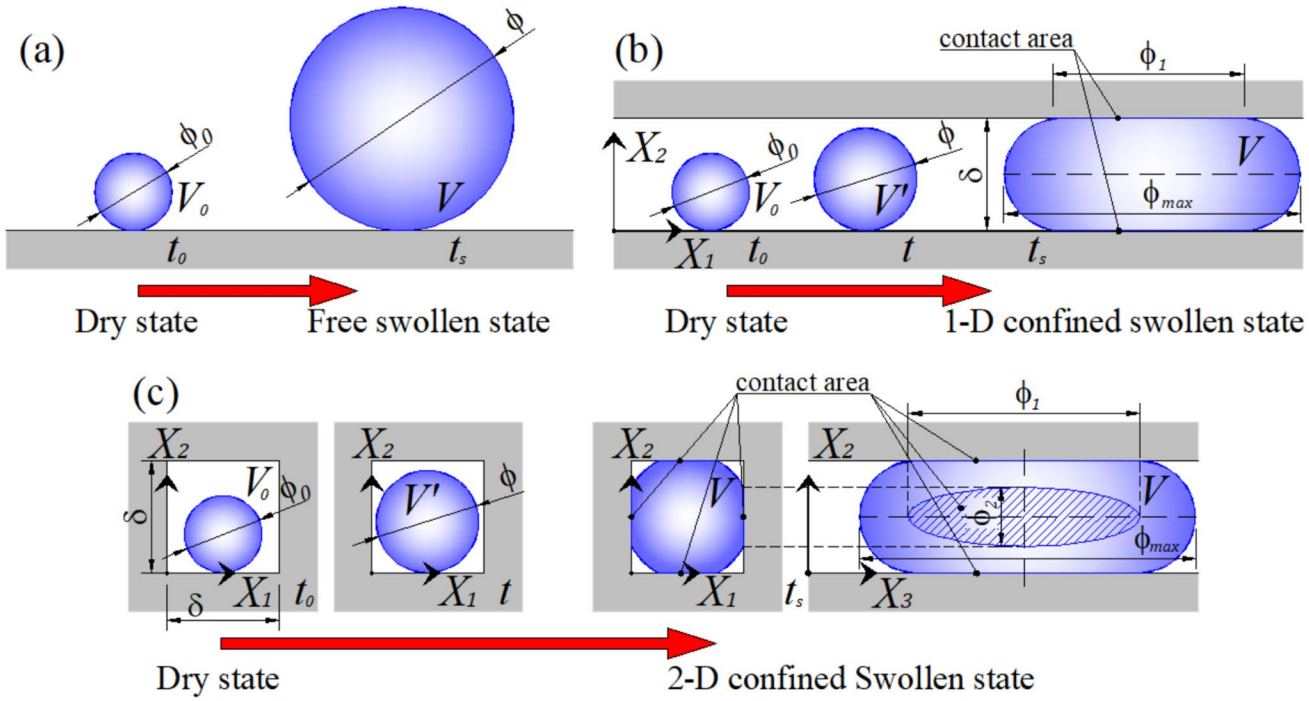

Fig. 2 Free (**a**), 1D constrained swelling (**b**), and 2D constrained swelling (**c**) of an hydrogel having an initial (dry) spherical shape with diameter ϕ_0 and volume V_0. Upon swelling, the volume increases up to the steady state condition at time t_s reaching the final volume V

where $F()$ is a non-linear dimensionless function depending on the material's constitutive law and problem geometry [36, 37]; the above expression reduces to the classical Hertzian contact equation for not too large deformations [38]: $P = \frac{E}{3(1-\nu^2)}\phi^2\left(\frac{u}{\phi}\right)^{3/2}$. The latter relationship will be used to experimentally determine the Young's modulus of the gel in the steady swollen state, i.e. at complete swelling, by adopting as usual $\nu = 1/2$, and considering not too large deformations, as occurs at the beginning of the contact phenomenon considered in the experimental tests.

4 Experimental tests

4.1 Free swelling

We performed both free and constrained swelling tests of hydrogel beads, having nearly a spherical shape in the dry state, made of poly(acrylamid-co-acrylic acid) with side groups – CONH2 and – COOH. Upon submersion in water, the beads swell and increase their volume several times. For each considered test, five beads were used to determine the average and the standard deviation of the quantities of interest, such as the volume ratio, the gel-rigid surface contThe initial average diameter of the beads in their dry state is $\phi_0 = 4.99 \pm 0.09mm$, while their initial dry mass is equal to $m_0 = 0.106 \pm 0.008g$. Upon reaching the steady state of swelling, mechanical compression tests have been conducted to determine the elastic properties of the hydrogel using of Eq. (1). Figure 3 shows the shear modulus *vs* the diametral stretch of spherical hydrogel elements under compression; an average value falling in the range $G = 9.5 - 12kPa$ can be reasonably adopted for the studied gel; in the following, the average value $G = 10.75kPa$ is adopted.

act stress, etc.

 https://doi.org/10.1007/s11012-026-02095-6

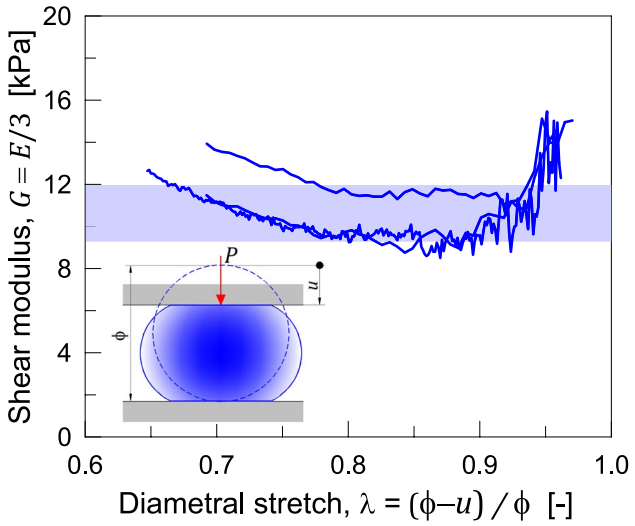

Fig. 3 Shear modulus vs the diametral stretch of the gel sphere during compression mechanical tests. The average shear modulus falls within the interval 9.5–12 kPa

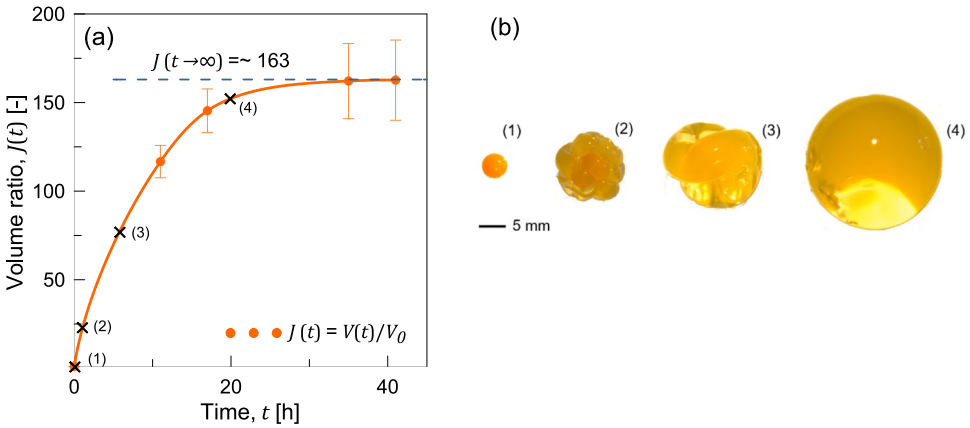

Fig. 4 Free swelling of a spherical hydrogel bead immersed in water. Volume ratio vs time (**a**). Swollen configurations at different time instants (**b**): 0 h (1), 1.5 h (2), 6 h (3), 20 h (4)

In order to assess the degree of swelling, quantified through the volume ratio J, the amount of water entered into the hydrogel beads' network is determined by weight measurements at regular time intervals. The equilibrium condition, corresponding to the variational condition stated by Eq. (4), attained for a sufficiently long time of immersion in water for which the volume ratio J is known, enables the evaluation of the interaction parameter χ of the gel as will be shown in the following.

In free swelling conditions, the gel beads initially swell showing an irregular shape due to the growth of unstable modes in response to local differential swelling in the material [39, 40]. In Fig. 4b, the shape evolution of the gel during swelling is shown.

Since in free swelling $\boldsymbol{F} = J^{1/3}\mathbf{1}$, by using the well-known relationship $\boldsymbol{\sigma} = J^{-1}\frac{\partial \Psi_{net}(\boldsymbol{F})}{\partial \boldsymbol{F}}\boldsymbol{F}^T$, where Ψ_{net} is expressed by Eq. (6), the stress state in the gel's network at the swollen steady state can be found to be characterized by the hydrostatic (tensile) stress $p = 11.41kPa$ (referred to the current configuration), i.e. $\boldsymbol{\sigma} = p \cdot \mathbf{1}$ (or equivalently $\boldsymbol{P} = \frac{\partial \Psi_{net}(\boldsymbol{F})}{\partial \boldsymbol{F}} = \boldsymbol{p} \cdot \mathbf{1}$, with $\boldsymbol{p} = 340.53kPa$ in the reference dry configuration) while the deformation gradient tensor is expressed by $\boldsymbol{F} = \lambda \cdot \mathbf{1}$, with $\lambda = 5.463$.

4.2 Confined swelling

In the second series of tests, the hydrogel beads are forced to swell in a confined environment consisting in 3D printed PLA plates limiting the expansion of the gel during swelling. Both 1-D and 2-D confinements have been considered (see Fig. 1b, c): in the first case, two stiff (rigid) planes, placed at a relative distance δ equal to 10, 15, and 18 *mm*, surround the gel in order to prevent its expansion more than the above-mentioned distances in a single direction. In the second case, the gel beads are forced to swell in a rigid tube with a square cross-section having sizes 10, 15, and 18 *mm*, respectively.

The initial average diameter of the beads in their dry state for the three above-considered 1-D confinements are: a) $\phi_0 = 4.87 \pm 0.13mm$, $m_0 = 0.096 \pm 0.010g$ (confinement $\delta = 10mm, \delta/\phi_0 = 2.05$), b) $\phi_0 = 5.01 \pm 0.07mmm_0 = 0.101 \pm 0.004g$ (confinement $\delta = 15mm, \delta/\phi_0 = 2.99$), c) $\phi_0 = 4.98 \pm 0.06mmm_0 = 0.104 \pm 0.004g$ (confinement $\delta = 18mm, \delta/\phi_0 = 3.61$). As for the 2-D confinements, the initial characteristics of the gel beads are the following: a) $\phi_0 = 4.77 \pm 0.02mm, m_0 = 0.093 \pm 0.054g$ (confinement $\delta = 10mm, \delta/\phi_0 = 2.09$), b) $\phi_0 = 4.93 \pm 0.01mmm_0 = 0.098 \pm 0.057g$ (confinement $\delta = 15mm, \delta/\phi_0 = 3.04$), c) $\phi_0 = 4.92 \pm 0.01mmm_0 = 0.099 \pm 0.057g$ (confinement $\delta = 18mm, \delta/\phi_0 = 3.66$). According to the above-reported average diameters of the dry gel beads, the three confinements are approximately characterized by the relative size ratios $\delta/\phi_0 = 2.0;3.0;3.6$, respectively.

The volume ratio J is calculated by weighing the hydrogel at regular time intervals, after taking out the swollen beads from their confining environment for a very short time (less than 2 min). The experimentally measured evolution of the volume ratio with its relative standard deviation, is shown in Fig. 4 for the case of free swelling, while the volume ratio of the two above-illustrated confined swelling conditions is shown in Fig. 5.

It is worth noticing that in one case (2-D confinement of 10 *mm* the test was interrupted after about 18 h because of the failure of most of the tested gel beads. From the minimum condition of the total energy density, $\psi_{gel} = \psi_{net}(\boldsymbol{F}) + \psi_{mix}(C_s) + \psi_p(J, C_s)$, it is possible to evaluate the Flory–Huggins interaction parameter for the various considered cases; in particular, a numerical procedure that, by varying χ, iteratively searches for the minimum of the total energy density $\psi_{gel} = \psi_{net}(\boldsymbol{F}) + \psi_{mix}(C_s) + \psi_p(J, C_s)$ for a given known volume ratio J, has been used.

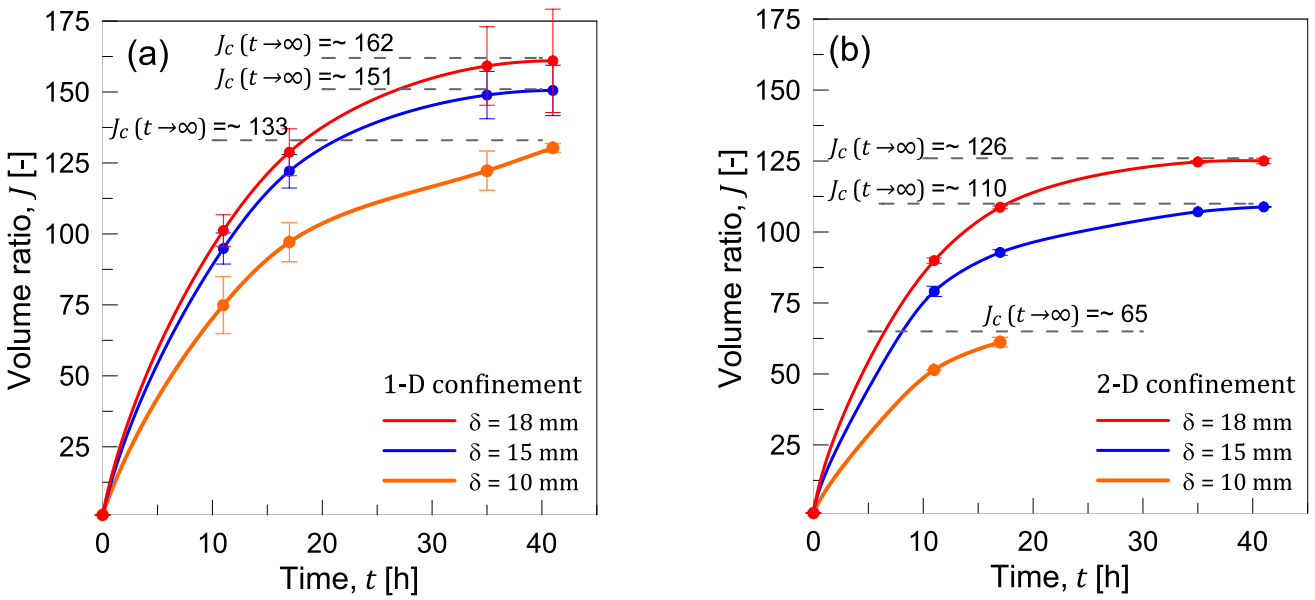

Fig. 5 Confined swelling of a spherical hydrogel bead immersed in water. volume ratio vs time for the 1-D and 2-D confined swelling. The steady state volume ratio for confined swelling J_c is also indicated. Measurements have been performed at the time instants corresponding to the dot symbols, while continuous lines are the interpolation of the test data

 https://doi.org/10.1007/s11012-026-02095-6

Table 1 Flory–Huggins interaction parameter χ estimated from experimental tests in the steady state condition for the free and for the 1-D and 2-D confined swelling cases. In the bottom lines, the water concentrations C_s per unit initial dry gel volume (expressed in $[mol/m^3]$) are also reported

Confinement	$\delta = 10mm$	$\delta = 15mm$	$\delta = 18mm$	*Free swelling*
1-D	$\chi = 0.257$ $C_s = 7.33 \cdot 10^6 mol/m^3$	$\chi = 0.201$ $C_s = 8.33 \cdot 10^6 mol/m^3$	$\chi = 0.160$ $C_s = 8.94 \cdot 10^6 mol/m^3$	$\chi = 0.155$ $C_s = 9.00 \cdot 10^6 mol/m^3$
2-D	$\chi = 0.431$ $C_s = 3.55 \cdot 10^6 mol/m^3$	$\chi = 0.325$ $C_s = 6.05 \cdot 10^6 mol/m^3$	$\chi = 0.280$ $C_s = 6.94 \cdot 10^6 mol/m^3$	

The determined values are reported in Table 1 (by neglecting the temperature effect that does not play any role for the class of the considered hydrogels) where it can be appreciated that the limitation to the volume expansion of the hydrogel obtained by applying the 1-D and 2-D confinements, corresponds to a fictitious increase of the effective interaction parameter χ of the gel; the more the gel is confined, the more the interaction parameter increases, indicating a mechanically-induced lower network-fluid affinity. In the same table, the solvent concentration in the various cases has been evaluated by considering that for water $v_s = 1.801 \cdot 10^{-5} m^3/mol$ (Fig. 5).

The hydrogel-rigid plane contact area has been observed at regular time intervals for the two series of confinements. In Figs. 6, 7 some exemplary images of the contact area for the 1-D confinement (Fig. 6) and for the 2-D one (Fig. 7) are shown (Table 1).

For the 1-D confinement case, once the hydrogel spheres initiate to be in contact with the rigid planes, the immersion in water was briefly suspended and a mechanical test was conducted at regular time intervals to determine the compressive force P necessary to recover the above-mentioned fixed distance of the applied constraint. The average contact stress $\sigma_0 = P/A$ was obtained by considering the contact area A between the gel

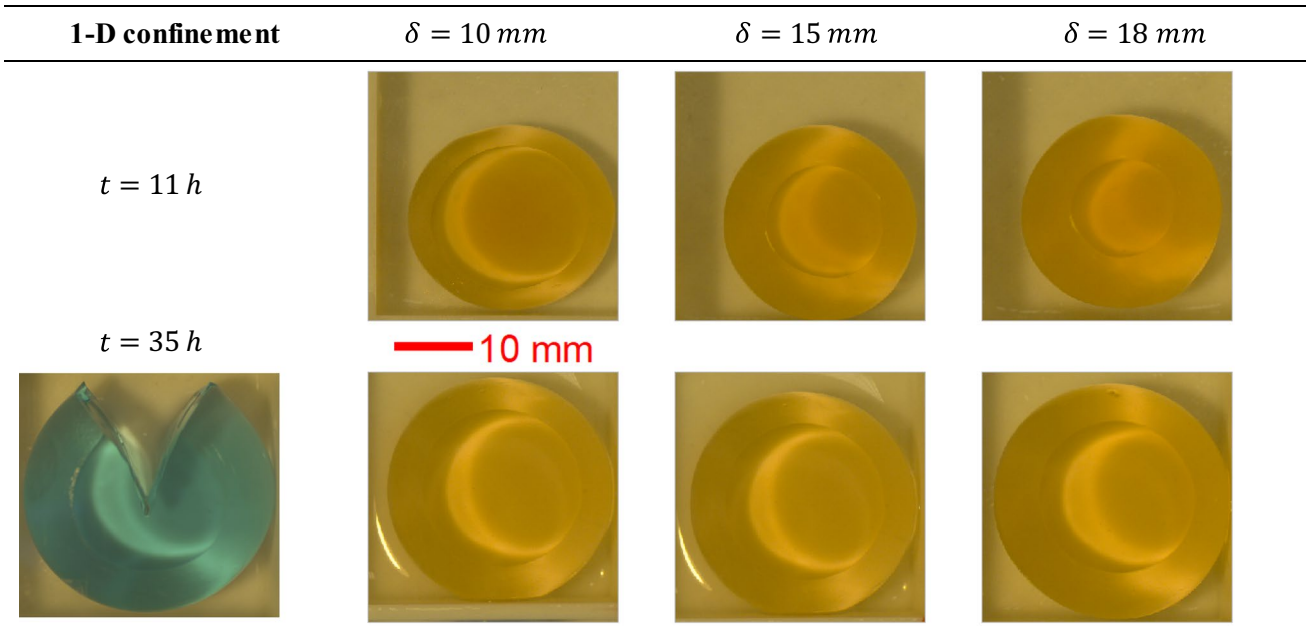

Fig. 6 Top views of 1-D confined swelling for three different confinements at the time instants $t = 11h$ and $t = 35h$ of immersion in water. In some cases, the hydrogel bead undergoes fracture as can be observed from the left hand side picture; the fracture surface appears to be roughly normal to the two confining planes

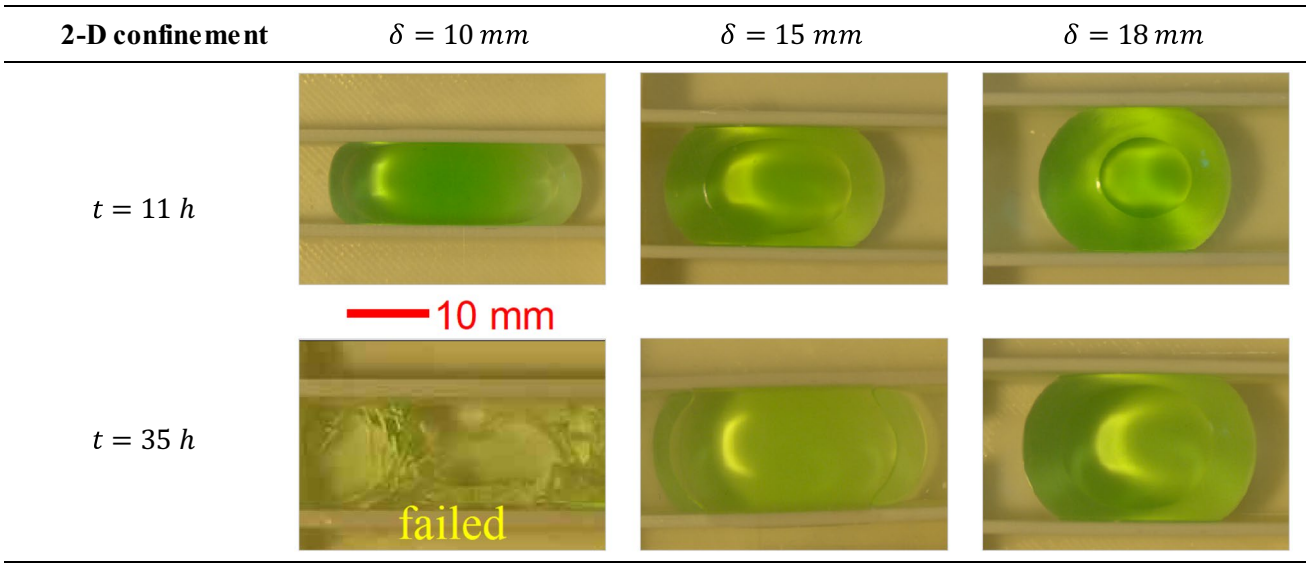

Fig. 7 Lateral views of 2-D confined swelling for three different confinements at the time instants $t = 11h$ and $t = 35h$ of immersion in water

and the rigid contact (transparent) plane, measured through high-resolution pictures of the confined gel at various time instants of the swelling process (Fig. 8).

The average contact stress σ_0 increases by decreasing the confinement distance δ and such an increase becomes more pronounced for longer swelling times. For sake of completeness, the real contact stress distribution $\sigma(r)$ provided by contact mechanics theory [41], compared to the average one σ_0, is shown in the detail of Fig. 8b.

In the confined steady swollen states, once the volume ratio J_c is known, the network stretches in the coordinate directions $\lambda_1, \lambda_2, \lambda_3$—here assumed to be roughly homogeneous throughout the gel domain—can be easily determined; the corresponding deformation gradient tensors become:

$$\begin{aligned} \boldsymbol{F}_{1-D} &= \begin{bmatrix} \sqrt{J_c/F_{22}} & 0 & 0 \\ 0 & \delta/\phi_0 & 0 \\ 0 & 0 & \sqrt{J_c/F_{22}} \end{bmatrix} \\ \boldsymbol{F}_{2-D} &= \begin{bmatrix} \delta/\phi_0 & 0 & 0 \\ 0 & \delta/\phi_0 & 0 \\ 0 & 0 & J_c/(F_{11}F_{22}) \end{bmatrix} \end{aligned} \tag{8}$$

for the 1-D and 2-D confinements, respectively. Let's indicate with $\boldsymbol{P}_{1-D}$ and $\boldsymbol{P}_{2-D}$ the corresponding 1st Piola–Kirchhoff stress tensors obtained by differentiating the network energy density with respect to the deformation gradient tensor. On the other hand, the deformation gradient tensors in the case of isotropic swelling (taking place in absence of any constraint) with the same volume ratio J_c are:

$$\boldsymbol{F}_{1-D}\big|_{iso} = J_c^{1/3}\mathbf{1},\ \boldsymbol{F}_{2-D}\big|_{iso} = J_c^{1/3}\mathbf{1} \tag{9}$$

with the corresponding 1st Piola–Kirchhoff stress tensors, $\boldsymbol{P}_{1-D}\big|_{iso}$ and $\boldsymbol{P}_{2-D}\big|_{iso}$.

The stress applied by the gel to the confining surfaces can thus be roughly estimated as the difference between the two above-mentioned 1st Piola–Kirchhoff stress tensors; in other words, it represents the stress required to bring the gel from the isotropically swollen state to the confined one, both characterized by the same volume ratio J_c, i.e.:

 https://doi.org/10.1007/s11012-026-02095-6

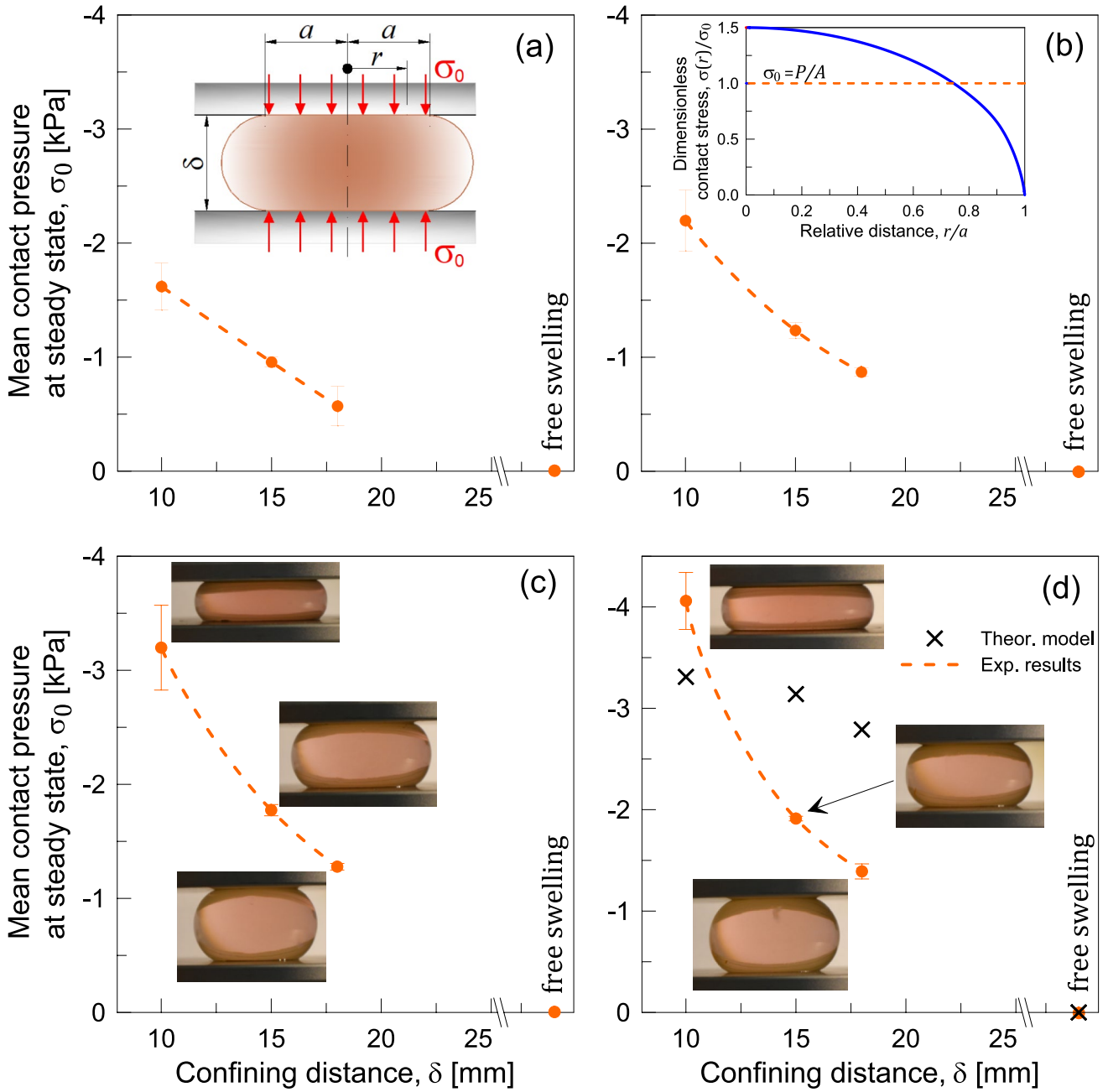

Fig. 8 Mean contact pressure σ_0 between the gel and the contact surface in 1-D confined swelling vs the confining distance δ. Mean contact pressure after 11 h (**a**), 17 h (**b**), 35 h (**c**), and 41 h (**d**). The comparison between the average contact stress and the real one [41] provided by contact mechanics theory is illustrated in the insert of sub-figure (**b**). The symbols a and r represent the radius of the contact area and the generic distance from the center of the circular contact area

$$\boldsymbol{P}_{1-D}\big|_{contact} = \left(\boldsymbol{P}_{1-D}\big|_{iso} - \boldsymbol{P}_{1-D}\right),\ \boldsymbol{P}_{2-D}\big|_{contact} = \left(\boldsymbol{P}_{2-D}\big|_{iso} - \boldsymbol{P}_{2-D}\right) \tag{10}$$

while the corresponding confining surfaces' contact Cauchy stress tensors can be obtained as:

$$\boldsymbol{\sigma}_{1-D}\big|_{contact} = J_c^{-1}\boldsymbol{P}_{1-D}\big|_{contact}\boldsymbol{F}_{1-D}^{T},\ \boldsymbol{\sigma}_{2-D}\big|_{contact} = J_c^{-1}\boldsymbol{P}_{2-D}\big|_{contact}\boldsymbol{F}_{2-D}^{T} \tag{11}$$

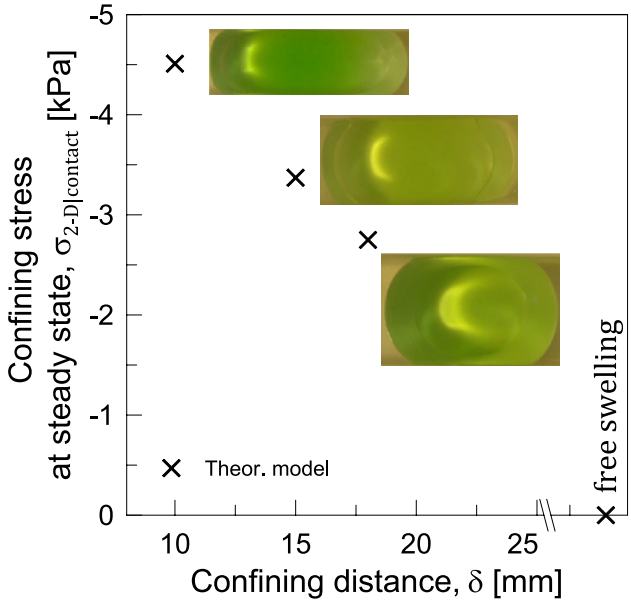

Fig. 9 Confining pressure σ_0 obtained from the theoretical model (see Eqs. 8–11) existing between the gel and the contact surface in 2-D confined swelling vs the confining distance δ at the steady state swelling condition

The confining contact stress obtained through the theoretical model is illustrated in Fig. 8d for the 1-D confinement and in Fig. 9 for the 2-D confinement. For the 1-D confinement, for which the experimental contact stress has been determined, the difference with the theoretical results is quite large, especially when the contact area has a limited extension such as in the case of $\delta = 15$ and $18mm$ since it is not correct to assume the contact stress to be homogeneously distributed inside the gel. For the 2-D confinement (Fig. 9), the experimental results have not been determined because of the complexity of a biaxial compression tests. From the simplified model, the confining stress $\boldsymbol{\sigma}_{2-D}\big|_{contact}$ decreases by increasing the confining distance; as discussed above, it has to be considered that such a stress is incorrectly overestimated by the model when the contact area has a limited extension compared to the transversal cross section of the gel domain.

The main source of inaccuracy of the proposed model is due to the lack of homogeneity in the stress state within the gel. The homogeneity of the stress state increases by increasing the degree of confinement (i.e. by decreasing the confining distance), so the theoretical model provides a better estimation of the contact stress for more severe confinements. According to the above discussion, a 2-D confinement is characterized by a more homogeneous stress state with respect to the 1-D case, so we expect that the theoretical model is more accurate in this latter case.

The contact Cauchy stress tensor can be additively decomposed into the hydrostatic and the deviatoric tensors as follows:

$$\boldsymbol{\sigma}_{1-D}\big|_{contact} = \mathbf{1}p_{1-D} + \boldsymbol{s}_{1-D},\ \ \boldsymbol{\sigma}_{2-D}\big|_{contact} = \mathbf{1}p_{2-D} + \boldsymbol{s}_{2-D} \tag{12}$$

In Fig. 10 the values of p and s_{22} obtained from the theoretical model are plotted vs the confining distance δ; it can be noticed that the hydrostatic stress p roughly changes by a factor of about 5 for large confining distance ($\delta = 18mm$) to a factor of 9 for small confining distance ($\delta = 10mm$), while the deviatoric stress component s_{22} changes by a factor 2 for large confining distance ($\delta = 18mm$) to a factor of about 7 for small confining distance ($\delta = 10mm$).

It is interesting to quantify the extension of the contact area in 1-D and 2-D confined swelling; in Fig. 11 the main sizes of the contact region described by the dimensionless distances $\phi_{max}/\phi_{sph}, \phi_1/\phi_{sph}$ in 1-D confined swelling, and $\phi_{max}/\phi_{sph}, \phi_1/\phi_{sph}, \phi_2/\phi_{sph}$ in 2-D confined swelling *vs* the confining distance δ at two time instants of swelling, namely 35 h for the 1-D confinement (Fig. 11a) and 11 h for the 2-D one (Fig. 11b) are illustrated. The size ϕ_{sph} indicates the diameter of the hydrogel element with a spherical shape having the same volume as the confined one.

 https://doi.org/10.1007/s11012-026-02095-6

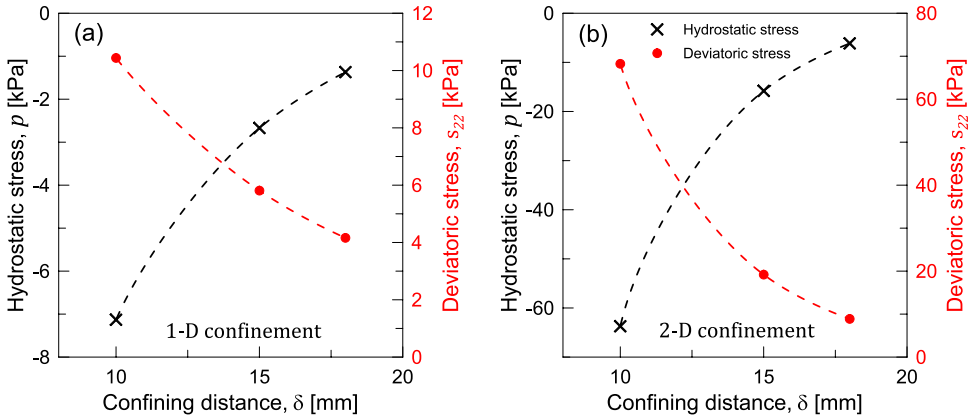

Fig. 10 Hydrostatic σ_p and deviatoric stress component s_{22} vs the confining distance δ, obtained from the theoretical model, for the 1-D (**a**) and 2-D (**b**) confinement at the steady state swelling condition

5 Conclusions

Swelling of hydrogels is a complex phenomenon—involving fluid diffusion, large deformation, hydrogen bond dissociation, chain entanglement, etc.—leading to a huge volume expansion of the polymer network. This physic-mechanical phenomenon can be controlled, such as in temperature-sensitive hydrogels or by changing the solvent fluid, in order to obtain a desired swelling degree. In this experimental study we have considered the case of mechanically controlled swelling obtained by using physical constraints. In particular, we have considered experimentally the swelling of poly(acrylamid-co-acrylic acid) hydrogels in free, 1-D, and 2-D different degrees of constrained conditions at various stages of swelling, and a theoretical interpretation has been provided. The volume ratio, the Flory–Huggins interaction parameter, the stress state in the gel network, and the contact stress with boundary walls in the considered conditions of confined swelling have been determined. A simple model to assess the contact stress of gel swelling in a 1-D and 2-D confined environment has been provided.

We have provided detailed quantitative information related to hydrogels swelling under 1-D and 2-D confinements; understanding how the swelling process takes place in presence of rigid boundaries, what is the gel-confinement contact pressure, as well as the contact area evolution, represent fundamental information for the tuning and designing of gel-based smart and active devices.

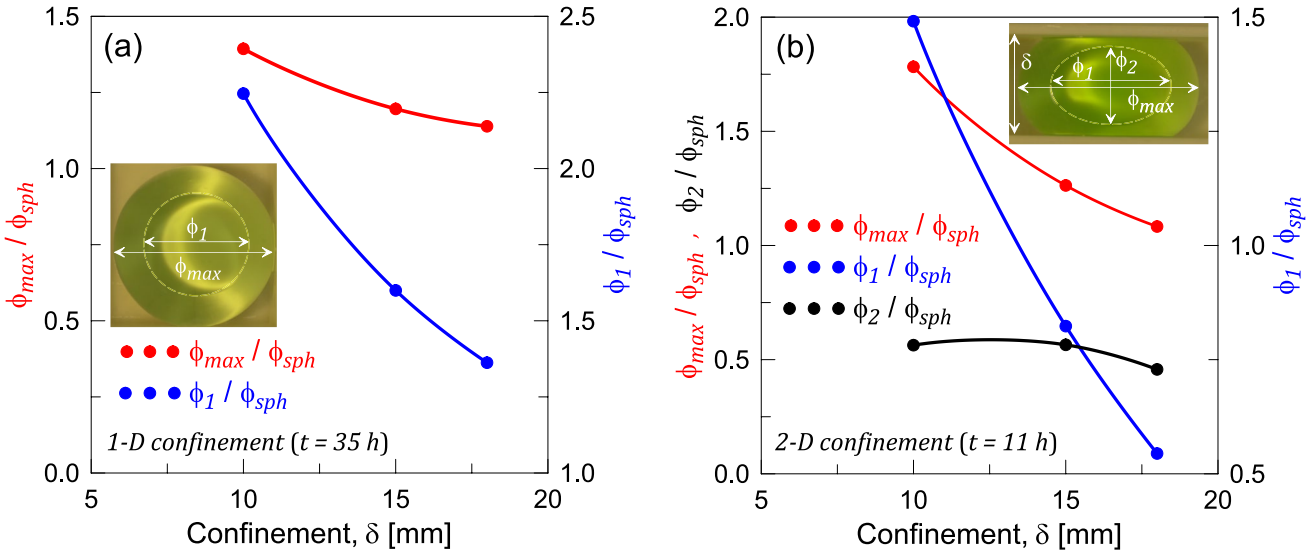

Fig. 11 Dimensionless contact sizes arising in 1-D (**a**) and 2-D (**b**) confined swelling. ϕ_{sph} is the diameter of the sphere having the same volume of the swollen gel at the considered time

Although similar cases have been explored in the scientific literature, the present results provide a useful contribution to quantify the effect of different confinement types and degrees, as well as the contact pressure generated by hydrogels swelling under constraints. These results are useful to improve the knowledge on the quantitative behavior of hydrogels swelling in free and confined conditions. The swelling degree and the mechanical pressure exerted during the confined swelling, is fundamental in various applications such as chemo-mechanical sensing, drug delivery, tissue engineering, soft robotics, cultural heritage conservation, etc. Controlled swelling and contact pressure exerted on a specific surface in confined swelling, might be used to activate sensor, operate soft actuators, release substances, trigger cleaning systems of works of art, etc.

Acknowledgements This project is supported by the Spoke 7 within the Italian National Research Programme (NRP)—PE05 (CHANGES), CUP: B53C22004010006.

Authors contributions SM performed the experimental analyses, collaborated in developing the modeling aspects, and revised the manuscript; FT revised the manuscript; MB revised the manuscript. RB conceived the research, developed the general modeling aspects, designed the experimental campaign and wrote the draft of the paper. All authors read and approved the final manuscript.

Funding Open access funding provided by Università degli Studi di Firenze within the CRUI-CARE Agreement. Italian National Research Programme, Spoke 7, PE05 (CHANGES), B53C22004010006, B53C22004010006.

Data availability Data related to the present research are available upon request to the authors.

Declarations

Conflict of interest The authors declare no competing interests.

References

1. Yang D (2022) Recent advances in hydrogels. Chem Mater 34(5):1987–1989
2. Wichterle O, Lìm D (1960) Hydrophilic gels for biological use. Nature 185:117–118
3. Rezakhani L, Gharibshahian M, Salehi M, Zamani S, Abpeikar Z, Ghaderzadeh O, Cheraghali D (2024) Recent advances in hydrogels applications for tissue engineering and clinical trials. Regen Ther 26:635–645
4. Chamkouri H, Chamkouri M (2021) A review of hydrogels, their properties and applications in medicine. Am J Biomed Sci Res 11(6):485–493
5. Wang R, Cheng C, Wang H, Wang D (2024) Swollen hydrogel nanotechnology: Advanced applications of the rudimentary swelling properties of hydrogels. ChemPhysMater. 3:357
6. Feng W, Wang Z (2023) Tailoring the swelling-shrinkable behavior of hydrogels for biomedical applications. Adv Sci 10(28):2303326
7. Liu Z, Toh W, Ng TY (2015) Advances in mechanics of soft materials: a review of large deformation behavior of hydrogels. Int J Appl Mech 7(05):1530001
8. Brighenti R, Cosma MP (2022) Mechanics of multi-stimuli temperature-responsive hydrogels. J Mech Phys Solids 169:105045
9. Brighenti R, Li Y, Vernerey FJ (2020) Smart polymers for advanced applications: a mechanical perspective review. Front Mater 7:196. https://doi.org/10.3389/fmats.2020.00196

10. Cohen N (2019) Programming the equilibrium swelling response of heterogeneous polymeric gels. Int J Solids Struct 178:81–90
11. Webber JJ, Worster MG (2024) Wrinkling instabilities of swelling hydrogels. Phys Rev E 109(4):044602
12. Khaksar-Baghan N, Koochakzaei A, Hamzavi Y (2024) An overview of gel-based cleaning approaches for art conservation. Herit Sci 12(1):248
13. Spitz-Argolo MI, Sauer HI, Wunder RS, Petri J, Riegel-Vidotti IC (2025) Hydrogels from agar and citrus pectin for cleaning cultural heritage objects. J Mol Liq 431:127678
14. Chelazzi D, Baglioni P (2023) From nanoparticles to gels: a breakthrough in art conservation science. Langmuir 39(31):10744–10755
15. Vialetto J, Chelazzi D, Laurati M, Poggi G (2025) Exploring the combination of microgels and nanostructured fluids for the cleaning of works of art. Gels 11(6):382
16. Mastrangelo R, Guaragnone T, Casini A, Bandelli D, Chelazzi D, Baglioni P (2025) "Twin-chain" hydrogels with tailored porosity, surface roughness, and cleaning capabilities. Langmuir 41(16):10238–10249
17. Casini A, Chelazzi D, Baglioni P (2023) Advanced methodologies for the cleaning of works of art. Sci China Technol Sci 66(8):2162–2182
18. Highley CB, Song KH, Daly AC, Burdick JA (2019) Jammed microgel inks for 3D printing applications. Adv Sci 6(1):1801076
19. Lin G, Chang S, Kuo CH, Magda J, Solzbacher F (2009) Free swelling and confined smart hydrogels for applications in chemomechanical sensors for physiological monitoring. Sens Actuators B Chem 136(1):186–195
20. Plummer A, Adkins C, Louf JF, Košmrlj A, Datta SS (2024) Obstructed swelling and fracture of hydrogels. Soft Matter 20(7):1425–1437
21. Levin M, Cohen N (2023) Swelling under constraints: exploiting 3D-printing to optimize the performance of gel-based devices. Adv Mater Technol 8(14):2202136
22. Vernerey F, Shen T (2017) The mechanics of hydrogel crawlers in confined environment. J R Soc Interface 14(132):20170242
23. Wu F, Pang Y, Liu J (2020) Swelling-strengthening hydrogels by embedding with deformable nanobarriers. Nat Commun 11(1):4502
24. Monchetti S, Brighenti R, Hanuhov T, Cohen N (2024) Controlled swelling-induced shape change of soft gel filled structures. Thin-Walled Struct 204:112280
25. Flory PJ (1942) Thermodynamics of high polymer solutions. J Chem Phys 10:51–61. https://doi.org/10.1063/1.1723621
26. Flory PJ, Rehner J (1943) Statistical mechanics of cross-linked polymer networks II. Swelling. J Chem Phys 11:521–526
27. Flory PJ (1950) Statistical mechanics of swelling of network structures. J Chem Phys 18:108–111
28. Huggins ML (1964) A revised theory of high polymer solutions. J Am Chem Soc 86:3535–3540. https://doi.org/10.1021/ja01071a028
29. Tanaka T, Fillmore DJ (1979) Kinetics of swelling of gels. J Chem Phys 70:1214–1218
30. Doi M (2009) Gel dynamics. J Phys Soc Jpn 78:052001
31. Hong W, Zhao X, Zhou J, Suo Z (2008) A theory of coupled diffusion and large deformation in polymeric gels. J Mech Phys Solids 56:1779–1793
32. Cai S, Suo Z (2011) Mechanics and chemical thermodynamics of phase transition in temperature-sensitive hydrogels. J Mech Phys Solids 59:2259–2278
33. Marcombe R, Cai S, Hong W, Zhao X, Lapusta Y, Suo Z (2010) A theory of constrained swelling of a pH-sensitive hydrogel. Soft Matter 6(4):784–793
34. Doi M (1996) Introduction to polymer physics. Oxford University Press
35. Doi M (2013) Soft matter physics. Oxford University Press, USA
36. Liu DX, Zhang ZD, Sun LZ (2010) Nonlinear elastic load–displacement relation for spherical indentation on rubberlike materials. J Mater Res 25(11):2197–2202
37. Giannakopoulos AE, Triantafyllou A (2007) Spherical indentation of incompressible rubber-like materials. J Mech Phys Solids 55(6):1196–1211
38. Johnson K (1987) Contact Mechanics. Cambridge University Press
39. Barros W, de Azevedo EN, Engelsberg M (2012) Surface pattern formation in a swelling gel. Soft Matter 8(32):8511–8516
40. Bertrand T, Peixinho J, Mukhopadhyay S, MacMinn CW (2016) Dynamics of swelling and drying in a spherical gel. Phys Rev Appl 6(6):064010
41. Ding Y, Niu XR, Wang GF (2015) Elastic compression of nanoparticles with surface energy. J Phys D Appl Phys 48(48):485303

Authors and Affiliations

Silvia Monchetti[1] · Farzad Tatar[2] · Michele Betti[1] · Roberto Brighenti[1]

✉ Roberto Brighenti
roberto.brighenti@unifi.it

[1] Department of Civil and Environmental Engineering, University of Florence, Via Di S. Marta 3, 50199 Florence, Italy

[2] Department of Engineering and Architecture, University of Parma, Parco Area Delle Scienze 181/A, 43124 Parma, Italy